

Article

Changes in the Fluorescence of Biological Particles Exposed to Environmental Conditions in the National Capitol Region

Joshua L. Santarpia ^{1,*†‡}, Don R. Collins ^{2,§}, Shanna A. Ratnesar-Shumate ^{3,†‡}, Crystal C. Glen ¹, Andres L. Sanchez ¹, Carlos G. Antonietti ², Jilliane Taylor ^{2,||}, Nathan F. Taylor ^{2,||}, Christopher A. Bare ³, Sean M. Kinahan ^{3,†‡}, Danielle N. Rivera ^{1,†‡}, Elizabeth Corson ^{3,¶}, Steven C. Hill ^{4,||}, Chatt C. Williamson ⁴, Mark Coleman ^{4,**} and Yong-Le Pan ⁴

¹ Sandia National Laboratories, 1611 Innovation Pkwy SE, Albuquerque, NM 87123, USA

² Department of Atmospheric Sciences, Texas A&M University, College Station, TX 77843, USA

³ Applied Physics Laboratory, Johns Hopkins University, 11100 Johns Hopkins Road, Laurel, MD 20723, USA

⁴ DEVCOM-Army Research Laboratory, 2800 Powder Mill Rd., Adelphi, MD 20783, USA

* Correspondence: josh.santarpia@unmc.edu

† Current address: Department of Pathology and Microbiology, University of Nebraska Medical Center, Omaha, NE 68198, USA.

‡ Current address: National Strategic Research Institute, Omaha, NE 68106, USA.

§ Current address: Chemical and Environmental Engineering, University of California, Riverside, Riverside, CA 92521, USA.

|| Current address: U.S. Environmental Protection Agency, Dallas, TX 75270, USA.

¶ Current address: Department of Computer Science, Johns Hopkins University, Baltimore, MD 21218, USA.

** Retired.



Citation: Santarpia, J.L.; Collins, D.R.; Ratnesar-Shumate, S.A.; Glen, C.C.; Sanchez, A.L.; Antonietti, C.G.; Taylor, J.; Taylor, N.F.; Bare, C.A.; Kinahan, S.M.; et al. Changes in the Fluorescence of Biological Particles Exposed to Environmental Conditions in the National Capitol Region. *Atmosphere* **2022**, *13*, 1358. <https://doi.org/10.3390/atmos13091358>

Academic Editors: Salvatore Romano and Martin Gallagher

Received: 21 July 2022

Accepted: 22 August 2022

Published: 25 August 2022

Publisher's Note: MDPI stays neutral with regard to jurisdictional claims in published maps and institutional affiliations.

Abstract: A variety of methods have been used to study atmospheric bioaerosols. A common technique employed for the detection and measurement of bioaerosols is the measurement of the autofluorescence of biological particles when excited by ultraviolet light. We examined the changes in the fluorescence spectra of bioaerosols when exposed to ambient outdoor conditions for periods of several hours. The bioaerosols in this study were contained in a Captive Aerosol Growth and Evolution (CAGE) chamber that employed two rotating drums constructed with an exterior FEP Teflon film to allow sunlight to penetrate and an inner ePTFE membrane to allow ambient trace gasses to permeate the drums. The bioaerosols were periodically measured with a TSI UV-APS (excited at 355 nm) and a single-particle fluorescence spectrometer (excited at 351 and 263 nm). The data indicate changes in both fluorescence spectral profile and intensity from *Bacillus thuringiensis* var. *kurstaki* spores and MS2 bacteriophage particles during the experiments. The changes observed in these particles appear to be due to a combination of the environmental conditions rather than attributable to any single factor. The results of this study indicate that bioaerosols are significantly altered by atmospheric aging processes and that these changes may affect measurements by ultra-violet light induced fluorescence (UV-LIF) or other spectroscopic techniques.

Keywords: bioaerosols; atmospheric aging; trace gasses



Copyright: © 2022 by the authors. Licensee MDPI, Basel, Switzerland. This article is an open access article distributed under the terms and conditions of the Creative Commons Attribution (CC BY) license (<https://creativecommons.org/licenses/by/4.0/>).

1. Introduction

The detection and characterization of ambient biological particles is relevant to many scientific fields, including human health [1–3], the atmospheric water cycle such as cloud condensation or ice nuclei [4], biological defense [5], and the characterization of ambient microbiomes [6,7]. Traditional approaches to characterizing biological aerosol particles or bioaerosols involve the collection and analysis of viable or infectious microbes by culture and biochemical assays [5–7] and are limited by the lack of culturability of many environmental microbes [8].

Biological particles exposed to environmental conditions can undergo changes that impact their viability or infectivity [9–12]. Previous studies have indicated that microorganisms are susceptible to various environmental stresses. These environmental stresses include factors such as solar radiation, humidity, and chemical processes that result in secondary organic aerosol formation, often referred to as the open-air factor (OAF [9–13]). Changes in bioaerosols due to exposure to these environmental factors may impact the ability of some measurement techniques, i.e., ultra-violet light-induced fluorescence (UV-LIF [13–18]); polymerase chain reaction (PCR [19]); and protein detection such as immunoassays, to accurately measure the properties of ambient bioaerosols. These effects impact both the viability of atmospheric bioaerosols, as well as our ability to measure them by spectroscopic and molecular methods.

Few studies have attempted to investigate the impact of ambient conditions on the measurement of biological particles. Adhikari [20] examined seasonal variations in the concentration of pollen and fungal aerosols compared with ambient atmospheric conditions and found that temperature and ozone may influence those bioaerosol concentrations. Chi and Li [5] studied the size distribution and concentration of bioaerosols as a function of various pollutants and noted that bioaerosol concentration is impacted by solar radiation, relative humidity, and haze. Han [6] found that the concentration and size distribution of culturable fungi and bacteria correlated with the concentrations of SO₂, PM10, PM2.5, NO₂, and O₃; ambient temperature; and relative humidity. Chi [21] used fluorescent microscopy and microbial cultures to examine the relationships between meteorological factors, and culturable and non-culturable aerosols and reported strong correlations of the total bioaerosol content with temperature, rainfall, and solar radiation. Kowalski and Pastuszka [22] also found significant relationships between temperature and solar radiation on viable fungal and bacterial aerosol. Santarpia [23] noted that changes in relative humidity impacted the number of biologically fluorescent particles measured with a 405 nm excitation. Laboratory studies from Pecson et al. [24], Jung and Lee [25], and Schuit et al. [26] have demonstrated that UV radiation, electromagnetic radiation from microwaves, and thermal radiation from conventional heating have similar effects on the inactivation or decontamination of bacterial spores and bioaerosols of *B. anthracis*, *B. subtilis* and *B. thuringiensis*, the MS2 bacteriophage, and *E. coli*. Verreault et al. [27] and Peccia et al. [28] demonstrated the effects of relative humidity on the inactivation and optical properties of bioaerosols during UV irradiation and/or at high temperatures. Changes in bioaerosol properties in the natural environment involve many different chemical reactions that occur on multiple time scales (minutes, hours, and days) and may involve sequential reactions with one or multiple chemicals. For example, ozone not only modified the molecular structure and generated new chemicals by interacting with protein in bioaerosols but also resulted in the inactivation of bioaerosols and the loss of viability [29–31]. Alkanes, alkenes, aromatic hydrocarbons, and volatile organic compounds (VOCs) also react with bioaerosols via ozonolysis and photo-oxidation, etc. to change the properties of bioaerosols [32,33]. The results of these studies are indicative that ambient conditions (temperature, relative humidity, and solar radiation) and pollutant species (SO₂, NO₂, and O₃) influence measured bioaerosol concentrations. The complexity of the atmospheric conditions complicate the study of bioaerosol property in the outdoor environment, as reviewed by Šantl-Temkiv et al., and there are many challenges in performing research in this field [34].

In the present study, an outdoor chamber designed to allow ambient environmental factors including solar radiation, relative humidity, temperature, and trace gasses to penetrate its interior was used to study the changes in aerosolized bacteria (*Bacillus thuringiensis* var. *kurstaki*) and viruses (the MS2 bacteriophage) at a site located near a highway in the National Capitol Region. The chamber design integrated the concepts of ambient smog [35,36] and rotating drum chambers (e.g., Goldberg [37]) to retain micron-sized biological particles suspended as aerosols for several hours for observation outdoors.

2. Materials and Methods

2.1. CAGE System

The Captive Aerosol Growth and Evolution (CAGE) chamber system (Figure 1; [38]) is a rotating and sun-tracking chamber system that was designed to study the evolution of aerosols under conditions identical or similar to those of the surrounding atmospheric environment. The system consists of two chambers, each constructed from three concentric, thin-film cylinders. The system was designed to rotate in order to keep super-micron particles aloft for hours [15–17,19,39–41]. At each end of the chambers are inlets and outlets connected by rotary unions that allow for the introduction and sampling of particles or gas-phase species. The chamber walls are constructed of fluorinated ethylene propylene (FEP) Teflon, which is transparent to natural solar radiation [36] and is chemically inert. The cylinder end-caps are constructed of a gas-permeable expanded polytetrafluoroethylene (ePTFE) membrane to allow for gas exchange between the inside of the chamber and the local ambient environment. This chamber system allowed for aging of the bioaerosols directly outdoors in the ambient environment while maintaining the particles aloft in the chambers for several hours.

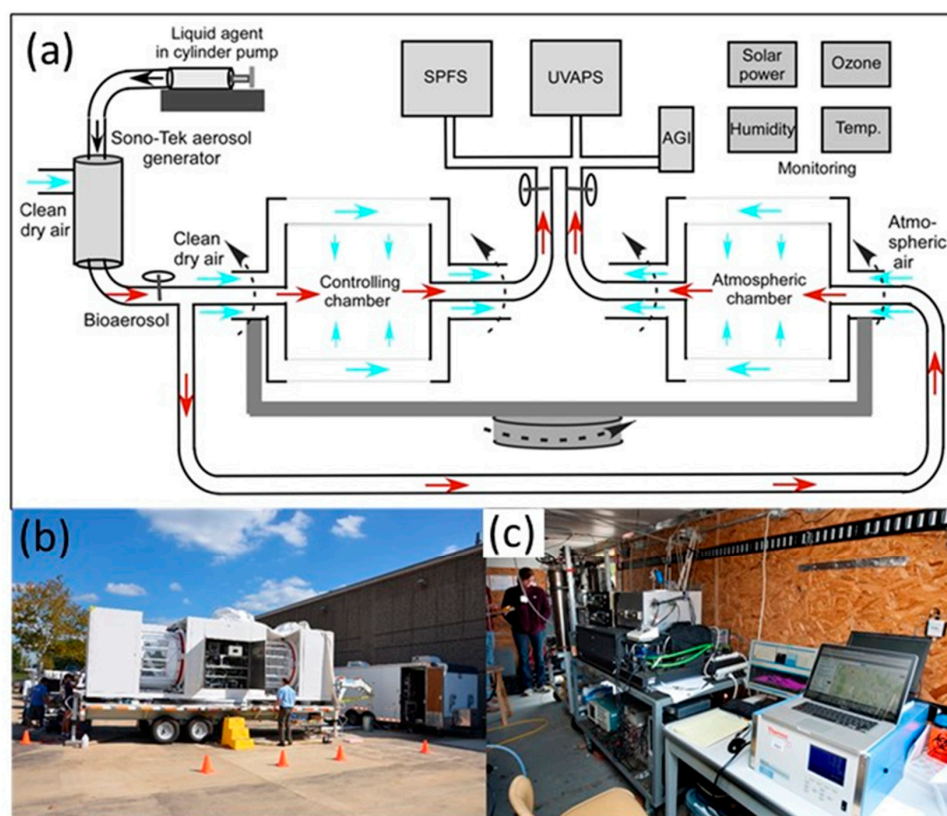


Figure 1. (a) Diagram (top) and (b) photographs (bottom left) of the Captive Aerosol Growth and Evolution (CAGE) chamber system used in this study. (c) The aerosol generator, the single-particle fluorescence spectrometer (SPFS), the ozone analyzer, and the precision spectral pyrometer, etc. controlling and measuring devices (the bottom right photograph) within the truck trailer sitting at the right side of the bottom left photograph.

During this study, experiments were conducted for up to seven hours, with the platform rotating to track the sun [38]. Although a second control chamber was a part of this design, only a single chamber, the atmospheric chamber (Figure 1a), was used to generate these data, which allowed particle-filtered ambient air to be exchanged with the chamber air. Throughout the experiments, the chamber rotated at approximately 1 rpm. The chamber configuration used only two of the three chamber walls: the reactor volume

and the outer insulating volume. The recirculating blowers ran in the outer volume, and a controlled vacuum that maintained the reactor volume bag taut under negative pressure was applied.

2.2. Experimental Design

The fluorescence of MS2 and *Bacillus thuringiensis* var. *kurstaki* (*Btk*) aerosol particles was measured during the month of October during 2012 in the CAGES chambers in Adelphi, MD (39.029–76.966). Measurements of *Btk* were made on 3–5 October 2012. Two separate experiments were performed on 3 October 2012: one in the morning (08:50–13:15 LT) and one in the afternoon (15:35–20:06 LT). One complete measurement was made on 4 October 2012 (10:48–19:55 LT), and another was made on 5 October 2012 (09:15–13:07 LT). Measurements of MS2 aerosol particle fluorescence were carried out on 15 October 2012 (09:05–18:00 LT), 16 October 2012 (09:00–16:00 LT), 17 October 2012 (09:25–18:15 LT), and 18 October 2012 (09:05–17:30 LT).

2.3. Preparation, Enumeration, and Generation of Bioaerosols

2.3.1. Btk Spores

The *Btk* spores were generously provided by Dugway Proving Grounds for this study. The spores were rehydrated to a concentration of 1 mg/mL in 0.22 µm sterile-filtered deionized water to produce a target particle size of approximately 2 µm. This stock suspension was vortexed for two minutes and refrigerated until utilized for the experiments. The resulting aerosol suspension concentration was approximately 8×10^5 CFU/mL.

The bacterial stocks were enumerated in triplicate by plating on Tryptic Soy Agar (TSA) plates using a Spiral Biotech Autoplate (50 µL exponential setting) and incubated overnight (sixteen hours) at 37 °C. A Spiral Biotech Q-Count calculated the number of colonies and the resulting concentration.

2.3.2. MS2

The male-specific bacteriophage (MS2, ATCC 15597-B1, American Type Culture Collection, Gaithersburg, MD, USA) production and plaque assays utilized *Escherichia coli* str. C-3000 (*E. coli* ATCC 15597, American Type Culture Collection, Gaithersburg, MD, USA) as the host organism. The recommended medium, EM 271, was prepared by combining and autoclaving 1% tryptone (BD 211705), 0.1% yeast extract (BD 212750), and 0.8% NaCl (Sigma S7653) (*w/v*). Agar (BD 214010) was added as a solid medium at 1.5%, and the resulting autoclaved medium was supplemented with 0.1% glucose (Sigma G5767, Sigma-Aldrich, Inc., St. Louis, MO, USA), 0.0294% CaCl₂ (Sigma C7902, Sigma-Aldrich, Inc., St. Louis, MO, USA), and 0.001% thiamine (Sigma T5941, Sigma-Aldrich, Inc., St. Louis, MO, USA) (*w/v*, sterile-filtered). *E. coli* C-3000 host cultures were propagated from glycerol stocks by overnight incubation on EM 271 agar at 37 °C. Individual colonies were harvested, placed into EM 271 broth, and incubated (37 °C, 200 RPM). Previously frozen MS2 stock was resuspended in EM 271, and 100 µL was used to inoculate the *E. coli* culture prior to the culture reaching the stationary growth phase. Incubation of the MS2 and *E. coli* suspension continued for eighteen hours. The overnight suspensions were harvested and diluted to 1:25 to produce a target particle size of approximately 2 µm for the aerosol experiments. The phage concentration was quantified by plaque assay prior to aerosolization. The concentration of the MS2 phage used in the experiments prior to aerosolization was approximately 8×10^9 PFU/mL.

The MS2 concentrations were determined by a plaque assay of stock serial dilutions, utilizing the same C-3000 strain of *E. coli*. Single colonies of *E. coli* were inoculated into EM 271 and incubated (37 °C, 200 RPM) until reaching the log-phase. The *E. coli* was co-inoculated with 0.5 mL of serially diluted MS2 into EM 271 containing 0.5% agar and was kept melted in a 46 °C water bath. The tube was then gently mixed, decanted onto EM 271 plates, and incubated overnight at 37 °C.

2.4. Aerosol Generation

The aerosol was generated using a 120 kHz ultrasonic spray nozzle (Sono-Tek, 06-04010, Sono-Tek Corporation, Milton, NY, USA), with a 30 mL syringe and pump (Sono-Tek, 11-01061) set to infuse the liquid suspension at a rate of 100 $\mu\text{L}/\text{min}$. The broadband ultrasonic generator (Sono-Tek, 06-05108) used to control the nozzle frequency and power was set to 3 W. The nozzle of the Sono-Tek was placed at the top of an aerosol capacitance chamber (ACC; [42]) to allow for mixing and initial evaporation of the droplets (initially 18 μm diameter) prior to them entering the CAGES. The aerosol was introduced into the CAGES from the ACC at a flow rate of 5 Lpm.

2.5. Aerosol Size, Concentration, and Fluorescence Measurement

A commercial UV-APS (UV-APS 3314, TSI, TSI Incorporated, Shoreview, MN, USA) was used to measure the aerodynamic particle size distribution and the integrated fluorescence intensity distribution (between 430 and 580 nm) when excited by a 355 nm laser. Sampling from the CAGES with the UV-APS was limited to 1 Lpm by attaching only the inner sample-flow inlet to the drum and letting the instrument pull the sheath air (4 Lpm) from the surrounding environment.

A single-particle fluorescence spectrometer (SPFS) [14,15,17] was used to measure the fluorescence spectra of individual bioaerosol particles from the CAGES system. The SPFS provides the dispersed fluorescence spectra from 280 to 560 nm excited by a 263 nm laser pulse, the dispersed fluorescence spectra from 380 to 650 nm excited by a 351 nm laser pulse, and an elastic scattering intensity resulting from illumination of a 685 nm laser for determining particle size. The fluorescence intensity for each particle was normalized for size by dividing by factors of $d^{2.05}$ (d is the diameter of the particle) for 263 nm excitation and $d^{2.8}$ for 351 nm excitation [14,17].

2.6. Ambient Environmental Measurements

During the experiments, ambient ozone and solar intensity were monitored on site using a 49i Ozone Analyzer (Thermo-Fisher, Thermo-Fisher, Lenexa, KS, USA) and a Precision Spectral Pyrometer (PSP, Epply Laboratory, Epply Laboratory, Newport, RI, USA). Relative humidity (RH), temperature, oxides of nitrogen (NO , NO_2 , NO_x , and NO_y), SO_2 , and UVB intensity data were obtained from Maryland Department of the Environment (MDE) from the Beltsville, MD, air-quality-monitoring site, located approximately 8 km northeast of the experiment site. The ozone concentration was recorded and either time-averaged between measurements to produce ozone concentration (ppb) on the same time scale as aerosol fluorescence measurements or integrated over the course of the experiment time to produce an integrated ozone concentration–time product (dose).

3. Results and Discussions

The average size distributions of the particles aerosolized into the CAGES, measured by the UV-APS, indicate that both the MS2 and *Btk* aerosols had mode diameters around 2.28 μm and geometric standard deviations between 1.3 and 1.4 (Figure 2). Data from two 7 h tests carried out on 4 October (*Btk*) and 17 October (MS2) demonstrate typical particle decay, as measured by the UV-APS observed in the CAGES during this study. The mean decay rate on October 4 was at $(0.20 \pm 0.03) \log_{10}(\text{particles}/\text{hour})$ and the mean decay rate on 17 October was $(0.22 \pm 0.02) \log_{10}(\text{particles})/\text{h}$.

Four experiments were conducted with *Btk*, in which dispersed fluorescence spectra from single *Btk* particles were collected along with ambient environmental data from local instruments and regional air-quality-monitoring stations. During this period, only a subset of the ambient data was available (temp, RH, NO_y , NO , O_3 , solar radiation, and UVB intensity). Fluorescence spectra were collected at regular intervals (approximately hourly) to examine their changes in the spectral profiles and intensities due to atmospheric aging of the particles over time. Representative spectra from the experiments performed on 4 October 2012 (Figure 3a,b) demonstrate a marked reduction in the fluorescence intensity across the entire

range of measured emission wavelengths for both excitation wavelengths at 263 nm and 351 nm. A similar decay in intensities was observed in all experiments. The UV fluorescence peak intensity around 330 nm was slightly blue-shifted during the aging process.

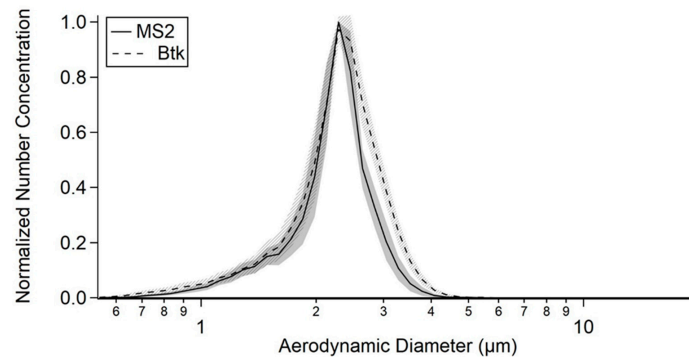


Figure 2. Normalized aerosol size distribution for MS2 (solid line) and *Btk* (dashed line) aerosol disseminated in this study. Shaded areas represent the standard deviation at each size. The means for *Btk* were calculated from experiments carried out on 3 and 4 October 2012, while the means for MS2 were calculated from experiments carried out on 15, 17 and 18 October 2012.

For experiments conducted with the MS2 phage, the fluorescence spectra were measured approximately hourly and exhibited significant reductions in intensity for both excitation wavelengths across a wide range of emission wavelengths (Figure 3c,d).

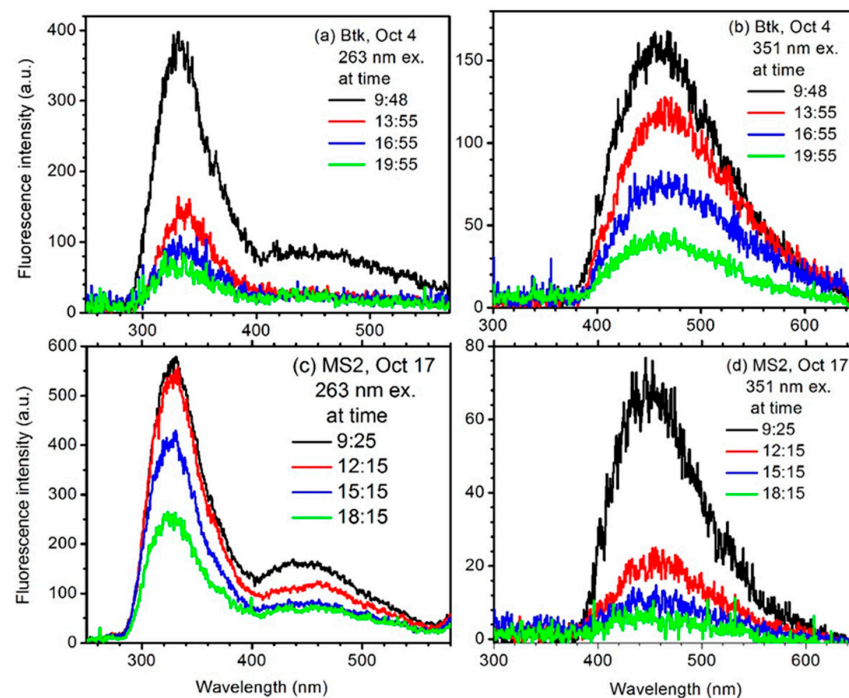


Figure 3. Representative wavelength resolved fluorescence spectra vs. time for *Btk* on 4 October 2012 (a,b) and MS2 on 17 October (c,d) at two excitation wavelengths: 263 nm (a,c) and 351 nm (b,d).

Fluorescence intensity was integrated into three emission bands (UV263, Vis263, and Vis351) and plotted versus time for all measurements for *Btk* (Figure 4) and MS2 (Figure 5). UV263 represents the integrated fluorescence intensity between 280 to 400 nm excited at 263 nm. Vis263 is the integrated fluorescence intensity between 400 to 580 nm excited at 263 nm. Vis351 is the integrated fluorescence intensity between 380 to 650 nm

excited at 351 nm. These integrated emission bands simplify the fluorescence intensity and spectral features so that the fluorescence data can be easily compared with the ambient environmental data. The temporal trends in the fluorescence bands generally decline in fluorescence intensity over the course of every experiment, as seen in Figures 4 and 5, although they have different decay rates and curves at different environmental conditions.

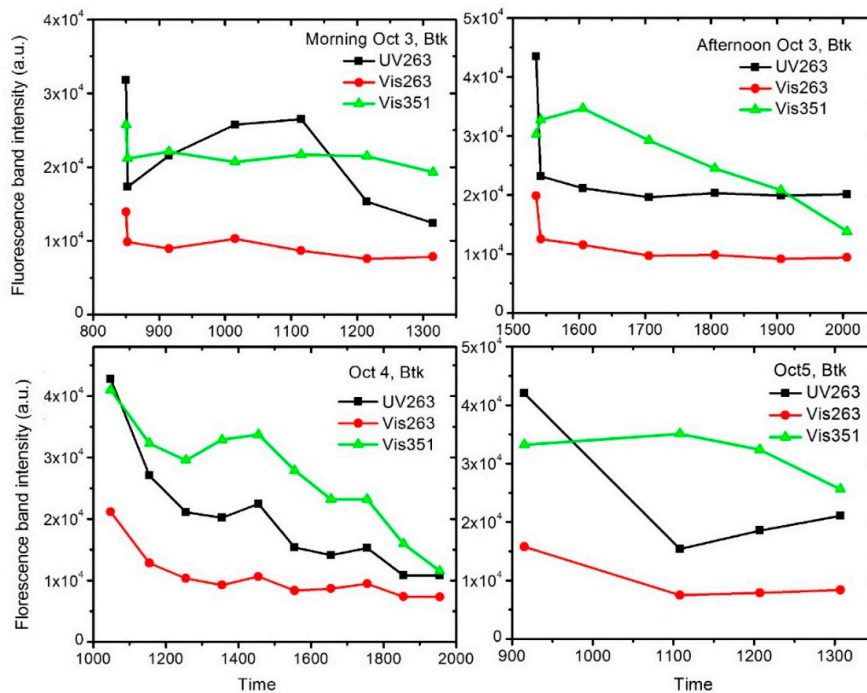


Figure 4. Changes in integrated fluorescence band intensities with time for *Btk* aerosol particles on 3 October (morning, top left; afternoon, top right), 4 October 2012 (bottom left), and 5 October 2012 (bottom right).

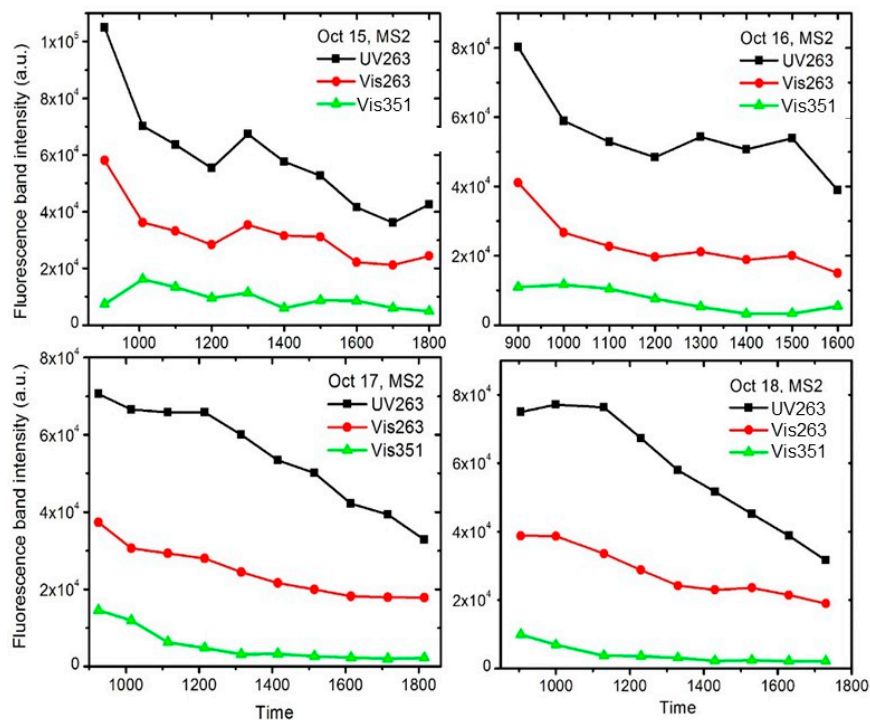


Figure 5. Changes in integrated fluorescence band intensities with time for MS2 aerosol on 15 October 2012 (top left), 16 October 2012 (top right), 17 October 2012 (bottom left), and 18 October 2012 (bottom right).

The strengths of the impacts of various ambient conditions on the three fluorescence bands of bioaerosols were investigated using Pearson's R values. These R values were calculated by pairing each fluorescence band with each ambient condition as a variable, as shown in Figure 6 for *Btk* and in Figure 7 for MS2. The ambient environmental conditions were either average hourly (the intensity) or integrated over time (the product of time and intensity, or the dose) to facilitate a comparison with the fluorescence bands. Therefore, each of the ambient factors shown on the horizontal axis in Figures 6 and 7 were either the average hourly intensity or the integrated dose over the time period between two fluorescence measurements (approximately 1 h). The doses of ozone, solar, and UVB radiation were integrated for comparison. The change rate of each fluorescence band ($d(\text{band intensity})/dt$) was calculated using a three-point finite difference scheme to facilitate comparisons with averaged and integrated ambient measurements.

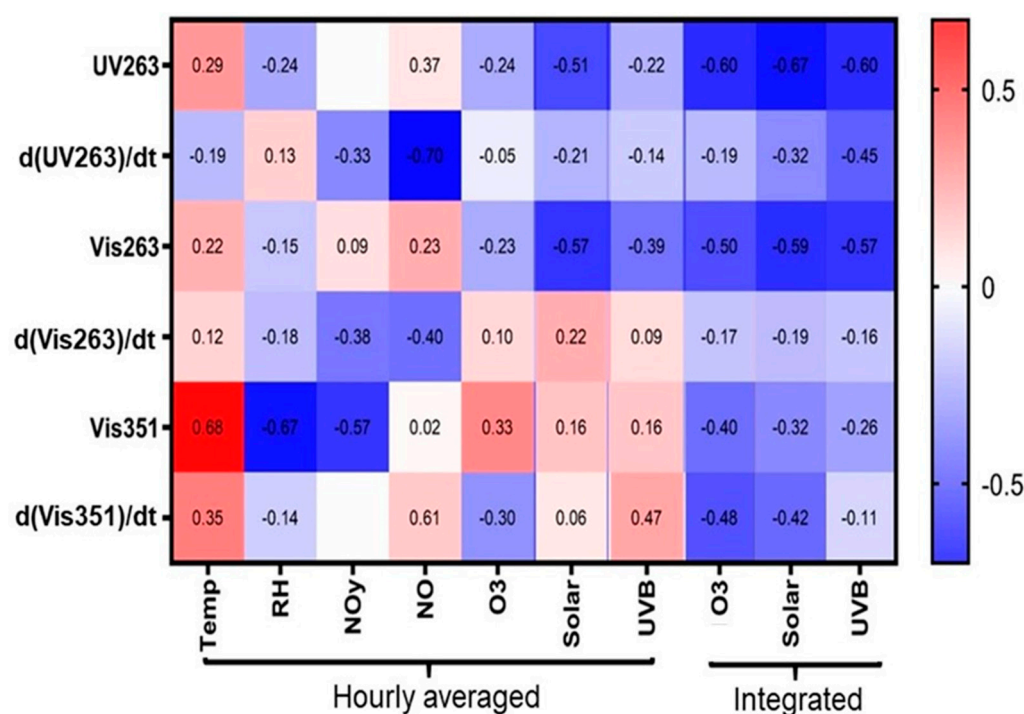


Figure 6. Heatmap of Pearson's R values showing positive (red) and negative (blue) correlations between the intensities of the three fluorescence bands and their first derivative (change rates), and the measured ambient conditions and pollutant levels for experiments involving *Btk* aerosol.

The patterns indicated by the Pearson's R value for each pairing is shown as a heatmap in Figures 6 and 7 with respect to each of the integrated fluorescence bands (UV263, Vis263, and Vis351) when paired with either the average environmental conditions or integrated O₃, solar, or UVB radiation. There are strong anticorrelations between the 263 nm excited fluorescence intensity (both UV263 and Vis263 bands) and the integrated ozone, total solar, and UVB radiation. In Figure 6 (*Btk*), these R vary from -0.6 to -0.67 for UV263 and from -0.5 to -0.59 for Vis263 band. In addition, moderate anticorrelations are observed for the Vis351 band with the three integrated conditions (R varying from -0.26 to -0.40); in contrast, the Vis351 band has slight to moderate correlations for the corresponding averaged conditions (R varying from 0.16 to 0.33). In Figure 7 (MS2), R varies from -0.71 to -0.83 for UV263 and from -0.71 to -0.81 for Vis263 band. This strong anticorrelation continues with the Vis351 band, where R varies from -0.75 to -0.86 , compared with the moderate anticorrelation for *Btk* in Figure 6 discussed above. However, the anticorrelations between the fluorescence and the average O₃, solar, or UVB radiation are generally much weaker, with a few notable exceptions, such as Vis351 with O₃ for MS2 ($R = -0.74$) and Vis263 with solar radiation for *Btk* ($R = -0.57$). UV263 and Vis263 on Oct 4 for *Btk* (Figure 4) and on

15–16 October for MS2 (Figure 5) showed near exponential decays in their aging processes upon the combined effects from all variables. Therefore, the relationships between the fluorescence and integrated O₃, total solar, or UVB radiation can be reasonably described by a linear model but not for the average values of the acting environmental conditions.

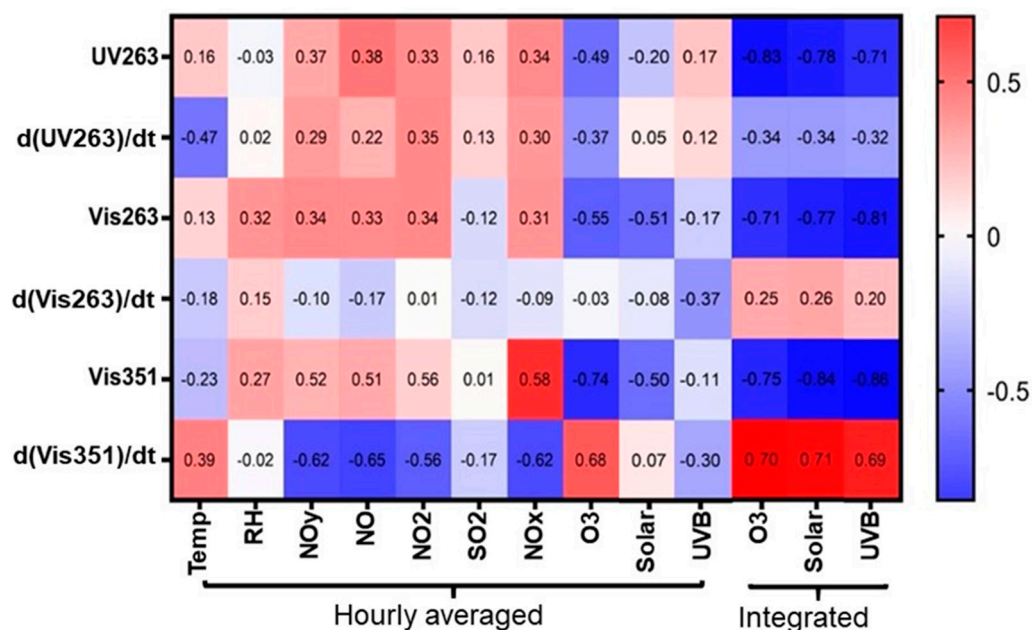


Figure 7. Heatmap of Pearson's R values showing positive (red) and negative (blue) correlations between the intensities of three fluorescence bands and their first derivative (change rates), and the measured ambient conditions and pollutant levels for experiments involving MS2 aerosol.

Due to the general collinearity between UVB, total solar, and O₃, these data cannot be used to definitively determine the specific role of any variable; however, a systematic check of all the relationships provides additional insights into the atmospheric aging mechanisms. Further close examination of the effects from the averaged ozone indicate that they are also anticorrelated with all fluorescence bands for MS2 (Figure 7) but appear correlated with the change rate of Vis351 ($d(\text{Vis351})/dt$). With *Btk* (Figure 6), the RH and NO_y also appear to have strong anticorrelations with the Vis351 band ($R = -0.67$ and -0.57 , respectively), while the change rate of Vis351 ($d(\text{Vis351})/dt$) is correlated with NO ($R = 0.61$). The average hourly solar intensity is anticorrelated with both fluorescence bands excited at 263 nm ($R = -0.51$ and -0.57 for UV263 and Vis263, respectively). Furthermore, the change rate of the UV263 band ($d(\text{UV263})/dt$) shows a significant anticorrelation with NO ($R = -0.70$). Visible fluorescence excited at 351 nm (Vis351) shows a strong correlation with temperature and an anticorrelation with RH. Generally, temperature and RH are anticorrelated.

The anticorrelation between fluorescence and integrated ozone, total solar, and UVB radiation is relatively strong. However, the rate of change in the Vis351 band ($d(\text{Vis351})/dt$) in MS2 appears to be strongly correlated with the averaged ozone intensity, integrated ozone, total solar, and UVB radiation ($R = 0.68$ – 0.71 ; Figure 7). This means that the Vis351 band intensity decreased increasingly slowly, while the doses of ozone, solar, or UVB radiation increased. Conversely, the Vis351 band is correlated with the oxides of nitrogen, with $R = 0.52$, 0.51 , 0.56 , and 0.58 for NO_y, NO, NO₂, and NO_x, respectively, while the change rate [$d(\text{Vis351})/dt$] is anticorrelated with the oxides of nitrogen, with $R = -0.62$, -0.65 , -0.56 , and -0.62 for NO_y, NO, NO₂, and NO_x, respectively.

Overall, the changes in *Btk* fluorescence observed were less well correlated with the environmental conditions than the changes in MS2. This is likely due to the differences between the particles. The aerosolized *Btk* particles had a mode size of 2 μm, mainly composed of spores. The spores likely have concentrations of fluorophores (such as tryptophan and

NADH) comparable with, or in the range of, those in vegetative cells. By contrast, the mass of 2 μm MS2 particles are likely composed of dried spent *E. coli* lysate and growth media, and much less viral mass, given the small size of the MS2 virus. The fluorescence is likely to be predominantly from the matrix, rather than from the virus. A quick calculation reveals that a 17 μm droplet generated by the Sonotek from the phage stock at $\sim 8 \times 10^9$ virions/mL that dries down to 2 μm likely contains about 20 MS2 viruses that make up only about 0.5% of the particle volume. This small fraction and previous work with lysates indicate that the lysate media is likely the dominant source of fluorescence, which is consistent with the previous observations [43]. Laboratory studies have also demonstrated that trace gasses impact the MS2 virus in this type of particle [14].

In general, the relationship between ozone and the decay in the UV fluorescence band (UV263) is likely explained by tryptophan ozonolysis–hydrolysis, which is consistent with the laboratory observations [14–18], especially with the high ambient humidity (e.g., RH above 40%) during all experimental times. The decay in the Vis351 band was likely due to the photodegradation by UVB (300 to 400 nm), which was the probable process causing the observed decrease in 351 nm excited fluorescence. Laboratory data [14–18] have also indicated that ozonolysis can increase the fluorescence intensity excited by 351 nm (Vis351). Although this process has been demonstrated in the laboratory, it appears that the changes observed in the Vis351 band in this study are likely dominated by photodegradation [13–18].

The atmospheric aging processes of bioaerosols, which are expressed here in averages of the measured two-wavelength excited fluorescence spectra of individual single bioaerosol particles, are much more complicated than the simple addition of the individual effects from each of the environmental conditions when the bioaerosol particles are exposed to the mixtures of reactive species (e.g., O_3 , NO, NO_2 , NO_x , NO_y , and SO_2) under various meteorological conditions (e.g., solar/UVB radiation, RH, and temperature). The induced changes, the mechanisms of change, and the rates of change can all be different due to different combinations of the environmental variables, including (1) which variables are present, (2) the intensities or concentration of each of the variables, and (3) the interaction times for each of them. Therefore, the correlations or anticorrelations between the intensities of fluorescence bands and the individual conditions presented in Figures 6 and 7 are only a very approximate representation of the complex relationships between the changes in the fluorescence of biological particles due to their exposure to environmental conditions and are far from a precise description of their combined effects. Although it is tempting to attempt to develop models of decay as a function of these variables, it is not possible to isolate the impacts of each variable without laboratory studies to investigate each variable and combinations of variables in a systematic way.

4. Conclusions

In September and October of 2012, experiments were conducted to investigate the changes in UV LIF spectra from MS2 and *Btk* aerosols in an outdoor Captive Aerosol Growth and Evolution (CAGE) chamber system consisting of two rotating drum chambers, into which the bioaerosols that were injected remained aloft inside and freely interacting with the surrounding atmospheric environments. Spectral changes in the UV LIF signatures of these particles over many hours along with measurements of the local environmental conditions (temperature, RH, NO_y , NO, O_3 , solar radiation, and UVB intensity) were observed. The results were analyzed using Pearson's R values, and some strong anticorrelations and correlations were found between the changes in fluorescence intensity and some environmental conditions, and the resulting mechanisms that may be responsible for the observed phenomena in UV LIF. This work provides a glimpse into some of the complex mechanisms that contribute to atmospheric aging processes for biological aerosols and provides a guide for additional laboratory studies. Such laboratory studies are needed to elucidate the mechanisms of decay needed to explain these observations.

Author Contributions: Conceptualization, J.L.S. and Y.-L.P.; Data curation, D.N.R. and Y.-L.P.; Formal analysis, J.L.S., S.A.R.-S. and Y.-L.P.; Funding acquisition, J.L.S., D.R.C. and Y.-L.P.; Investigation, J.L.S., D.R.C., S.A.R.-S., C.C.G., A.L.S., C.G.A., J.T., N.F.T., C.A.B., S.M.K., E.C., S.C.H., C.C.W., M.C. and Y.-L.P.; Methodology, J.L.S., D.R.C., S.A.R.-S., C.G.A. and Y.-L.P.; Software, C.C.W. and Y.-L.P.; Supervision, D.R.C., C.C.G. and Y.-L.P.; Visualization, J.L.S.; Writing—original draft, J.L.S., S.A.R.-S. and Y.-L.P.; Writing—review and editing, D.R.C., C.C.G., A.L.S., S.M.K., S.C.H. and C.C.W. All authors have read and agreed to the published version of the manuscript.

Funding: This research was supported by the Defense Threat Reduction Agency (DTRA) under contract number HDTRA1-10-C-0023 and by DEVCOM Army Research Laboratory mission funds.

Institutional Review Board Statement: Not applicable.

Informed Consent Statement: Not applicable.

Data Availability Statement: All data used in this manuscript can be found at <https://doi.org/10.17632/xppv4ypvhb.1>, accessed on 20 July 2022.

Conflicts of Interest: Santarpia is a paid consultant for both Inspirotec and Poppy Health, both of which develop and provide indoor infectious disease and allergen air-monitoring services and devices. All other authors report no conflicts of interest.

References

1. Möhler, O.; DeMott, P.J.; Vali, G.; Levin, Z. Microbiology and Atmospheric Processes: The Role of Biological Particles in Cloud Physics. *Biogeosciences* **2007**, *4*, 1059–1071. [[CrossRef](#)]
2. Beedham, R.J.; Davies, C.H. The UK Biological-Warfare Program: Dual-Use Contributions to the Field of Aerobiology. *Nonprolif. Rev.* **2021**, *27*, 309–322. [[CrossRef](#)]
3. Liu, D.; Mariman, R.; Gerlofs-Nijland, M.E.; Boere, J.F.; Folkerts, G.; Cassee, F.R.; Pinelli, E. Microbiome Composition of Airborne Particulate Matter from Livestock Farms and Their Effect on Innate Immune Receptors and Cells. *Sci. Total Environ.* **2019**, *688*, 1298–1307. [[CrossRef](#)] [[PubMed](#)]
4. Mazar, Y.; Cytryn, E.; Erel, Y.; Rudich, Y. Effect of Dust Storms on the Atmospheric Microbiome in the Eastern Mediterranean. *Environ. Sci. Technol.* **2016**, *50*, 4194–4202. [[CrossRef](#)] [[PubMed](#)]
5. Li, W.X.; Lu, R.; Xie, Z.S.; Wang, J.L.; Fan, C.L.; Liu, P.X.; Li, Y.P. Concentration and Size Distribution Characteristics of Culturable Bioaerosols at Various Air Quality Levels During Fall and Winter in Xi'an, China. *Huanjing Kexue/Environ. Sci.* **2017**, *38*, 4494–4500. [[CrossRef](#)]
6. Han, C.; Xie, M.; Qi, J.; Zhang, W.; Li, X.; Zhang, D. Size Distribution Characteristics of Culturable Bioaerosols in Relation to Air Quality Levels in Qingdao. *Res. Environ. Sci.* **2016**, *29*, 1264–1271. [[CrossRef](#)]
7. Santarpia, J.L. *Bioaerosols in the Environment: Populations, Measurement and Processes*; The Royal Society of Chemistry: London, UK, 2016.
8. Sharma, R.; Ranjan, R.; Kapardar, R.K.; Grover, A. “Unculturable” Bacterial Diversity: An Untapped Resource. *Curr. Sci.* **2005**, *89*, 72–77.
9. Cox, C.S.; Hood, A.M.; Baxter, J. Method for Comparing Concentrations of the Open-Air Factor. *Appl. Microbiol.* **1973**, *26*, 640–642. [[CrossRef](#)]
10. Hood, A.M. Open-Air Factors in Enclosed Systems. *J. Hyg.* **1974**, *72*, 53–60. [[CrossRef](#)]
11. Hood, A.M. The Effect of Open-Air Factors on the Virulence and Viability of Airborne. *Epidemiol. Infect.* **2009**, *137*, 753–761. [[CrossRef](#)]
12. Donaldson, A.I.; Ferris, N.P. The Survival of Foot-and-Mouth Disease Virus in Open Air Conditions. *J. Hyg.* **1975**, *74*, 409–416. [[CrossRef](#)] [[PubMed](#)]
13. Anthony Cox, R.; Ammann, M.; Crowley, J.N.; Griffiths, P.T.; Herrmann, H.; Hoffmann, E.H.; Jenkin, M.E.; Faye McNeill, V.; Mellouki, A.; Penkett, C.J.; et al. Opinion: The Germicidal Effect of Ambient Air (Open-Air Factor) Revisited. *Atmos. Chem. Phys.* **2021**, *21*, 13011–13018.
14. Pan, Y.-L.; Kalume, A.; Wang, C.; Santarpia, J. Atmospheric Aging Processes of Bioaerosols under Laboratory-Controlled Conditions: A Review. *J. Aerosol Sci.* **2021**, *155*, 105767. [[CrossRef](#)]
15. Ratnesar-Shumate, S.; Pan, Y.-L.; Hill, S.C.; Kinahan, S.; Corson, E.; Eshbaugh, J.; Santarpia, J.L. Fluorescence Spectra and Biological Activity of Aerosolized Bacillus Spores and MS2 Bacteriophage Exposed to Ozone at Different Relative Humidities in a Rotating Drum. *J. Quant. Spectrosc. Radiat. Transf.* **2015**, *153*, 13–28. [[CrossRef](#)]
16. Santarpia, J.L.; Pan, Y.-L.; Hill, S.C.; Baker, N.; Cottrell, B.; McKee, L.; Ratnesar-Shumate, S.; Pinnick, R.G. Changes in Fluorescence Spectra of Bioaerosols Exposed to Ozone in a Laboratory Reaction Chamber to Simulate Atmospheric Aging. *Opt. Express* **2012**, *20*, 29867–29881. [[CrossRef](#)]

17. Pan, Y.-L.; Hill, S.C.; Pinnick, R.G.; Santarpia, J.L.; Baker, N.; Alvarez, B.; Ratnesar-Shumate, S.; Cottrell, B.; McKee, L. Fluorescence Spectra of Bioaerosols Exposed to Ozone in a Laboratory Reaction Chamber to Simulate Atmospheric Processing. In Proceedings of the SPIE—The International Society for Optical Engineering, Orlando, FL, USA, 25–29 April 2011; Volume 8018.
18. Pan, Y.-L.; Santarpia, J.L.; Ratnesar-Shumate, S.; Corson, E.; Eshbaugh, J.; Hill, S.C.; Williamson, C.C.; Coleman, M.; Bare, C.; Kinahan, S. Effects of Ozone and Relative Humidity on Fluorescence Spectra of Octapeptide Bioaerosol Particles. *J. Quant. Spectrosc. Radiat. Transf.* **2014**, *133*, 538–550. [[CrossRef](#)]
19. Kinahan, S.M.; Tezak, M.S.; Siegrist, C.M.; Lucero, G.; Servantes, B.L.; Santarpia, J.L.; Kalume, A.; Zhang, J.; Felton, M.; Williamson, C.C.; et al. Changes of Fluorescence Spectra and Viability from Aging Aerosolized *E. coli* Cells under Various Laboratory-Controlled Conditions in an Advanced Rotating Drum. *Aerosol Sci. Technol.* **2019**, *53*, 1261–1276. [[CrossRef](#)]
20. Adhikari, A.; Reponen, T.; Grinshpun, S.A.; Martuzevicius, D.; Lemasters, G. Correlation of Ambient Inhalable Bioaerosols with Particulate Matter and Ozone: A Two-Year Study. *Environ. Pollut.* **2006**, *140*, 16–28. [[CrossRef](#)]
21. Chi, M.C.; Li, C.S. Fluorochrome in Monitoring Atmospheric Bioaerosols and Correlations with Meteorological Factors and Air Pollutants. *Aerosol Sci. Technol.* **2007**, *41*, 672–678. [[CrossRef](#)]
22. Kowalski, M.; Pastuszka, J.S. Effect of Ambient Air Temperature and Solar Radiation on Changes in Bacterial and Fungal Aerosols Concentration in the Urban Environment. *Ann. Agric. Environ. Med.* **2018**, *25*, 259–261. [[CrossRef](#)]
23. Santarpia, J.L.; Ratnesar-Shumate, S.; Gilberry, J.U.; Quizon, J.J. Relationship between Biologically Fluorescent Aerosol and Local Meteorological Conditions. *Aerosol Sci. Technol.* **2013**, *47*, 655–661. [[CrossRef](#)]
24. Pecson, B.M.; Martin, L.V.; Kohn, T. Quantitative PCR for Determining the Infectivity of Bacteriophage MS2 upon Inactivation by Heat, UV-B Radiation, and Singlet Oxygen: Advantages and Limitations of an Enzymatic Treatment to Reduce False-Positive Results. *Appl. Environ. Microbiol.* **2009**, *75*, 5544–5554. [[CrossRef](#)]
25. Jung, J.H.; Lee, J.E. Variation in the fluorescence intensity of thermally-exposed bacterial bioaerosols. *J. Aerosol Sci.* **2013**, *65*, 101–110. [[CrossRef](#)]
26. Schuit, M.; Ratnesar-Shumate, S.; Yolitz, J.; Williams, G.; Weaver, W.; Green, B.; Miller, D.; Krause, M.; Beck, K.; Wood, S.; et al. Airborne SARS-CoV-2 is Rapidly Inactivated by Simulated Sunlight. *J. Infect. Dis.* **2020**, *222*, 564–571. [[CrossRef](#)] [[PubMed](#)]
27. Verreault, D.; Marcoux-Voiselle, M.; Turgeon, N.; Moineau, S.; Duchaine, C. Resistance of Aerosolized Bacterial Viruses to Relative Humidity and Temperature. *Appl. Environ. Microbiol.* **2015**, *81*, 7305–7311. [[CrossRef](#)] [[PubMed](#)]
28. Peccia, J.; Werth, H.M.; Miller, S.; Hernandez, M. Effects of Relative Humidity on the Ultraviolet Induced Inactivation of Airborne Bacteria. *Aerosol Sci. Technol.* **2001**, *35*, 728–740. [[CrossRef](#)]
29. Kowalski, W.J.; Bahnfleth, W.P.; Whittam, T.S. Bactericidal Effects of High Airborne Ozone Concentrations on *Escherichia coli* and *Staphylococcus aureus*. *Ozone Sci. Eng.* **1998**, *20*, 205–221. [[CrossRef](#)]
30. Zhang, F.; Xi, J.; Huang, J.-J.; Hu, H.-Y. Effect of inlet ozone concentration on the performance of a micro-bubble ozonation system for inactivation of *Bacillus subtilis* spores. *Sep. Purif. Technol.* **2013**, *114*, 126–133. [[CrossRef](#)]
31. Clauss, M.; Linke, S.; Tautz, C.; Tautz, C.; Bromann, S. Development of a Novel Bioaerosol Chamber to Determine Survival Rates of Airborne Staphylococci. *Atmosphere* **2022**, *13*, 869. [[CrossRef](#)]
32. Chen, L.; Bao, K.; Li, K.; Lv, B.; Bao, Z.; Lin, C.; Wu, X.; Zheng, C.; Gao, X.; Cen, K. Ozone and Secondary Organic Aerosol Formation of Toluene/NO_x Irradiations under Complex Pollution Scenarios. *Aerosol Air Qual. Res.* **2017**, *17*, 1760–1771. [[CrossRef](#)]
33. Park, J.-H.; Babar, Z.B.; Baek, S.J.; Kim, H.S.; Lim, H.-J. Effects of NO_x on the molecular composition of secondary organic aerosol formed by the ozonolysis and photooxidation of α -pinene. *Atmos. Environ.* **2017**, *166*, 263–275. [[CrossRef](#)]
34. Šantl-Temkiv, T.; Sikoparija, B.; Maki, T.; Carotenuto, F.; Amato, P.; Yao, M.; Morris, C.E.; Schnell, R.; Jaenicke, R.; Pöhlker, C.; et al. Bioaerosol field measurements: Challenges and perspectives in outdoor studies. *Aerosol Sci. Technol.* **2020**, *54*, 520–546. [[CrossRef](#)]
35. Peng, J.; Hu, M.; Guo, S.; Du, Z.; Zheng, J.; Shang, D.; Levy Zamora, M.; Zeng, L.; Shao, M.; Wu, Y.-S.; et al. Markedly Enhanced Absorption and Direct Radiative Forcing of Black Carbon under Polluted Urban Environments. *Proc. Natl. Acad. Sci. USA* **2016**, *113*, 4266–4271. [[CrossRef](#)] [[PubMed](#)]
36. Paulsen, D.; Dommen, J.; Kalberer, M.; Prévôt, A.S.H.; Richter, R.; Sax, M.; Steinbacher, M.; Weingartner, E.; Baltensperger, U. Secondary Organic Aerosol Formation by Irradiation of 1,3,5-Trimethylbenzene–NO_x–H₂O in a New Reaction Chamber for Atmospheric Chemistry and Physics. *Environ. Sci. Technol.* **2005**, *39*, 2668–2678. [[CrossRef](#)]
37. Goldberg, L.J.; Watkins, H.M.S.; Boerke, E.E.; Chatigny, M.A. The Use of a Rotating Drum for the Study of Aerosols over Extended Periods of Time. *Am. J. Epidemiol.* **1958**, *68*, 85–93. [[CrossRef](#)]
38. Antonietti, C.G. Development of the Captive Aerosol Growth and Evolution Chamber System. Master’s Thesis, Texas A&M University, College Station, TX, USA, 2014.
39. Haddrell, A.E.; Thomas, R.J. Aerobiology: Experimental Considerations, Observations, and Future Tools. *Appl. Environ. Microbiol.* **2017**, *83*, e00809-17. [[CrossRef](#)]
40. Verreault, D.; Duchaine, C.; Marcoux-Voiselle, M.; Turgeon, N.; Roy, C.J. Design of an Environmentally Controlled Rotating Chamber for Bioaerosol Aging Studies. *Inhal. Toxicol.* **2014**, *26*, 554–558. [[CrossRef](#)]
41. Krumins, V.; Son, E.K.; Mainelis, G.; Fennell, D.E. Retention of Inactivated Bioaerosols and Ethene in a Rotating Bioreactor Constructed for Bioaerosol Activity Studies. *Clean Soil Air Water* **2008**, *36*, 593–600. [[CrossRef](#)]

42. Ratnesar-Shumate, S.; Wagner, M.L.; Kerechanin, C.; House, G.; Brinkley, K.M.; Bare, C.; Baker, N.A.; Quizon, R.; Quizon, J.; Proescher, A.; et al. Improved Method for the Evaluation of Real-Time Biological Aerosol Detection Technologies. *Aerosol Sci. Technol.* **2011**, *45*, 635–644. [[CrossRef](#)]
43. Pan, Y.-L.; Hill, S.C.; Santarpia, J.L.; Brinkley, K.; Sickler, T.; Coleman, M.; Williamson, C.; Gurton, K.; Felton, M.; Pinnick, R.G.; et al. Spectrally-Resolved Fluorescence Cross Sections of Aerosolized Biological Live Agents and Simulants Using Five Excitation Wavelengths in a BSL-3 Laboratory. *Opt. Express* **2014**, *22*, 8165–8189. [[CrossRef](#)]